RSC Advances

PAPER

View Article Online
View Journal | View Issue

Cite this: *RSC Adv.*, 2016, **6**, 16859

Nano iron pyrite (FeS_2) exhibits bi-functional electrode character†

Amarish Dubey,[a] Sushil Kumar Singh,[b] Brindan Tulachan,[c] Manas Roy,[d] Gaurav Srivastava,[c] Deepu Philip,[ae] Sabyasachi Sarkar‡[d] and Mainak Das‡*[ac]

Sustainable charge storage devices require materials that are environmentally benign, readily moldable, easily synthesizable, and profitable for applications in the electronics industry. Nano iron pyrite (FeS_2) is one such material, which is applicable in diverse areas like photovoltaic devices to seed dressing in agriculture. In this work, we propose an innovative application of nano FeS_2 *viz.*, as a symmetric charge storage device that is flexible, portable, and lightweight; along with its fabrication details. The device consists of a (H_3PO_4)/polyvinyl alcohol (PVA) electrolyte gel sandwiched between two similar electrodes made up of FeS_2/poly-aniline (PA), upon which graphite sheets are used as current collectors. Electrodes were characterized by XRD, FTIR and SEM. The device was calibrated by cyclic voltammetry and charge–discharge cycle. In its present laboratory prototype form, it powers solid-state electronic devices and electric motors. Further refinements of this device will open up new avenues in the field of sustainable charge storage devices and low power electronics.

Received 22nd January 2016
Accepted 2nd February 2016

DOI: 10.1039/c6ra01973k

www.rsc.org/advances

1. Introduction

There is an ever-increasing demand in the energy sector for compact, lightweight, portable, economical and environmental friendly charge storage devices. Charge storage devices are broadly classified as batteries, capacitors and super-capacitors.[1,2] The basic differences between these devices are in their energy storage potential, power density and cycle time.[3]

Current battery and super-capacitor manufacturers use a wide range of materials in combination. This includes sulfur-rich cathodes,[4] lithium polysulfide,[4] lithium nitrate,[5] sodium sulfide,[5] composite electrodes,[3,5–7] conducting polymers,[8] solid polymer electrolytes,[8–10] organic electrolytes[10,11] *etc.* Many of these materials are inherently toxic, highly reactive and cost prohibitive.[11,12] Thus there is always a quest for cheap, abundant and non-toxic materials for developing next generation of charge storage devices.[13–17]

Here we have developed a flexible, portable, light-weight charge storage device using nano iron pyrite (FeS_2). FeS_2 in its bulk form is an earth abundant mineral.[18–21] It is an environmentally benign compound.[21] It is readily and economically synthesized in nano-dimension, at a relatively low temperature.[22–24] Nano FeS_2 has been explored as a potential photovoltaic material and as a seed dressing agent in agriculture.[19,21–23,25] Nano FeS_2 has an effective electron density around 3×10^{18} cm^{-3}, intrinsic resistivity around 0.18 Ω cm, carrier mobility around 300 cm^2 V^{-1} s^{-1}, atomic packaging density around 7.55×10^{22} atoms per cm^3 and charge storage capacity of around 900 mA h g^{-1}.[18–21,26–28] Lithium ion battery manufacturers use it as a counter electrode.[29] In quest for cheap, abundant and non-toxic materials for developing next generation of charge storage devices,[13–17] we explore the possibility of developing a charge storage device using nano FeS_2. In this work, we are reporting the stepwise protocol for fabrication and characterization of a new kind of a flexible, symmetric charge storage device using nano FeS_2, where (FeS_2) exhibits bi-functional electrode character.

Why we used nano FeS_2? FeS_2 as such comprise of one electro-positive metal (Fe) with highly polarizable soft electro-negative sulfur atom. This will lead to a residual charge separation showing appreciable electro-positive character on iron and electro negative character on sulfur as well. Alignment of this charge distribution is selective, where if it function as a nucleophile then under a nano-surface the sulfur part will act as a nucleophile. Similarly its role of electrophile will be

[a]*Design Program, Indian Institute of Technology Kanpur, Kanpur, Uttar Pradesh, 208016, India. E-mail: amarish@iitk.ac.in; mainakd@iitk.ac.in; Fax: +91-512-259-4010; Tel: +91-512-259-4076*

[b]*Solid State Physics Laboratory, Defense Research Development Organization, Lucknow Road, Timar Pur, Delhi, 110054, India. E-mail: singhksushil@gmail.com*

[c]*Biological Sciences & Bioengineering, Indian Institute of Technology Kanpur, Kanpur, Uttar Pradesh, 208016, India. E-mail: tbrindan@iitk.ac.in; gsri@iitk.ac.in*

[d]*Department of Chemistry, Institute of Engineering Science and Technology, Shibpur, Botanic Garden, Howrah, West Bengal, 711103, India. E-mail: mroyiitk@gmail.com; abya@iitk.ac.in*

[e]*Industrial & Management Engineering, Indian Institute of Technology Kanpur, Kanpur, Uttar Pradesh, 208016, India. E-mail: dphilip@iitk.ac.in*

† Electronic supplementary information (ESI) available. See DOI: 10.1039/c6ra01973k

‡ SS and MD are co-corresponding authors.

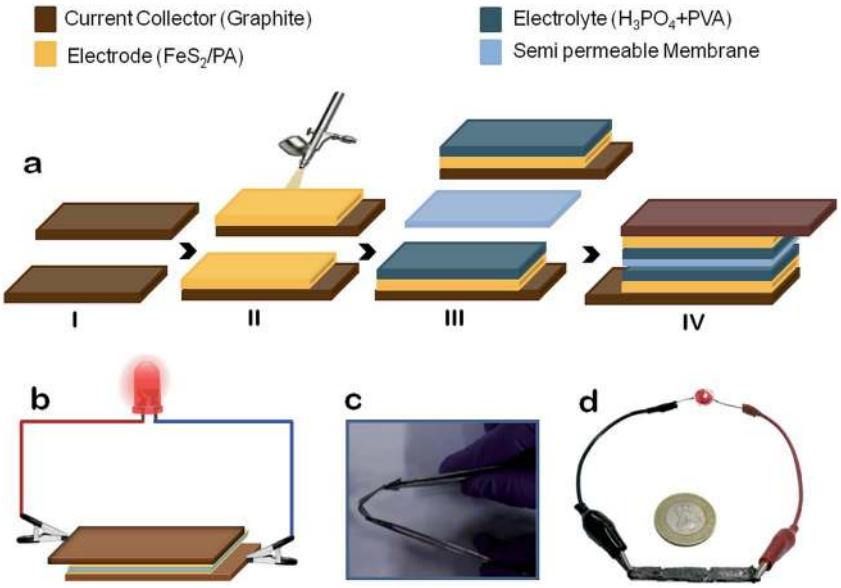

Fig. 1 Architecture and assembly of the prototyped charge storage device. (a) Preparation flow of charge storage device. (i) Two graphite sheets as current collectors. (ii) FeS_2/Poly-aniline composite spray painted using an air brush onto the graphite sheets for making the electrodes. (iii) The electrolyte gel (phosphoric acid + polyvinyl alcohol) is placed on top of the electrodes. (iv) Charge storage device assembly having a semi-permeable membrane between the gel faces. (b) A schematic representation of a functional charge storage device with symmetric nano FeS_2/PA electrodes connected to an LED. (c) Demonstrating flexibility property of the prototype. (d) Size comparison of actual charge storage device (three devices connected in series) with a standard coin.

automatically decided by the iron atom to embrace the approaching nucleophile. Thus under optimum condition an electrolyte can impose such polarization so that the two faces of nano FeS_2, may develop amphiphilic character. So a dissociable ionic electrolyte may allow its two ends, that is a cation and an anion to separate accordingly utilizing the nucleophilic and electrophilic heads of the nano FeS_2. Thus we propose that this unique feature of nano FeS_2 can be exploited to develop a bi-functional electrode to construct an electromotive cell. Fig. 1 describes the proposed device architecture.

2. Experimental section

2.1. Synthesis of FeS_2 nanoparticles

The major raw material for the device is nano iron pyrite. In this Section we described the nano FeS_2 synthesis. Multiple approaches are available for synthesis of FeS_2, where almost all of them require high temperature, yet few synthesis techniques utilize low temperature strategy.[22–24] A recent hot-injection based approach has successfully demonstrated FeS_2 synthesis at a temperature of 200 °C.[24] We developed a two-step method, which is slightly more complicated than the hot injection method, but can reduce the synthesis temperature to 100 °C. In the first step, we synthesized the polysulfide solution. In the second step, we use the polysulfide to synthesize the FeS_2 particles. Briefly the synthesis was based upon the nucleophilic reaction between polysulfide and $FeCl_3$ in an inert atmosphere at 100 °C, which resulted in the formation of FeS_2 nanoparticles with uniform morphology. During the course of this reaction, FeS and $FeSH^+$ species were formed, which reacted with polysulfide nucleophile thus leading to the formation of FeS_2.[22,23] The complete synthesis of nano FeS_2 is given in ESI section (Fig. S1†).

2.2. Electrolyte preparation and electrode fabrication

The synthesized nano FeS_2 particle powder color was grayish black. Now the base material is ready to make electrode material. So next, we developed the FeS_2/poly-aniline (PA) composite electrode by chemically polymerizing the monomers of aniline in the presence of FeS_2 nanoparticles in an aqueous suspension.[5] The detailed description of preparation is given in ESI and illustrated in Fig. S2.† After synthesis, we got the brownish precipitate, which was the composite of FeS_2 and poly-aniline (PA). PA electrodes were prepared by the same process as described above, without addition of FeS_2.[5,30,31] The electrolyte chosen for our charge storage device was a bio-compatible one, *viz.*, phosphoric acid (H_3PO_4). H_3PO_4 is a weak acid that disassociates into H^+ and $H_2PO_4^-$ ions. Poly-vinyl alcohol (PVA) was added to H_3PO_4 to create the polymeric-gel matrix that enables maximum entrapment of H_3PO_4 molecules; allowing ionic transportation with long time sustainability.[8–10] Gel electrolyte offers flexibility by retaining maximum fluid in its pores, thereby significantly reducing the evaporation rate; prolonging the functional life of the prototype. The detailed preparation schematic is provided in the ESI section (Fig. S2†).

2.3. Assembling the device

Fig. 1a details the assembly of the device. The outer current collectors are made of two identical graphite sheets, which are flexible, having high thermal and electrical conductivity,

possess chemical inertness, and has high refractory index. The dried FeS_2/PA which was synthesized for electrodes was deposited on one side of graphite sheets using spray painting guns. To facilitate the spraying process, 30 mg of FeS_2/PA was taken and mixed with 3 ml of isopropyl alcohol and 30 μl diluted (6×) Nafion solution, which was sonicated for four hours. The coating surface area was 2 cm^2 of the graphite sheets, as shown in Fig. 1a(i and ii). The electrolyte gel formed from phosphoric acid + polyvinyl alcohol gel (PVA/H_3PO_4) was poured and casted on top of the electrodes and left undisturbed for duration of four hours at a temperature around 25 °C. Two such electrodes and electrolyte assembly were prepared. Then these graphite sheets were assembled with the gel layers facing each other, while being separated by a cellulosic semi-permeable membrane, as shown in Fig. 1a(iii). The final assembly of the device is depicted in Fig. 1a(iv). Initially the device had no polarity, and it acquired its positive and negative terminals after its first charging. The terminal that was connected to the positive terminal of the source becomes positive and *vice versa*.

2.4. Structural characterization of the electrodes

The FeS_2/PA electrodes were characterized by X-ray diffraction (XRD), Fourier transform infrared spectroscopy (FTIR), Raman spectroscopy and scanning electron microscopy (SEM) techniques. XRD pattern of FeS_2 exhibited the diffraction peaks at 28.71, 33.05, 37.09, 40.73, 47.40, 56.18, 61.53 and 64.22; which were indexed to (111), (200), (210), (211), (220), (311), (222) and (023) planes respectively (Fig. 2a). This was consistent with single phase of FeS_2 (JCPDS card no. 42-1340) and indexed to space group *Pa*3 [205], that showed the cubic structure. No additional peak was observed in the XRD pattern thereby confirming the purity of the synthesized FeS_2 sample.[22,23,32–35] Similar peaks were observed in the diffraction pattern of FeS_2/PA, thus indicating that the while the polymerization of polyaniline took place, the FeS_2 particles were not dissolved in the acidic medium. By the Scherrer's equation ($D = K\lambda/B \cos\theta$), (where λ = wave length of X-ray, θ the diffraction angle, K the shape factor and $B = B_{actual} = \sqrt{(B_{observed}^2 - B_{resolution}^2)}$ is the correct half width of the observed half width) the average crystalline size was calculated to be 35 nm. In FTIR spectra (Fig. 2b), the FeS_2 powder exhibited a broad band centered at 3415 cm^{-1} and at 1615 cm^{-1}, which could be assigned to the O–H stretching and bending modes of water, respectively. The bands at 1420 cm^{-1} and 1355 cm^{-1} corresponds to the asymmetric S–O stretching of the sulfate species while the peaks at 612 cm^{-1} and 410 cm^{-1} were characteristic of the disulfide stretch (S–S).

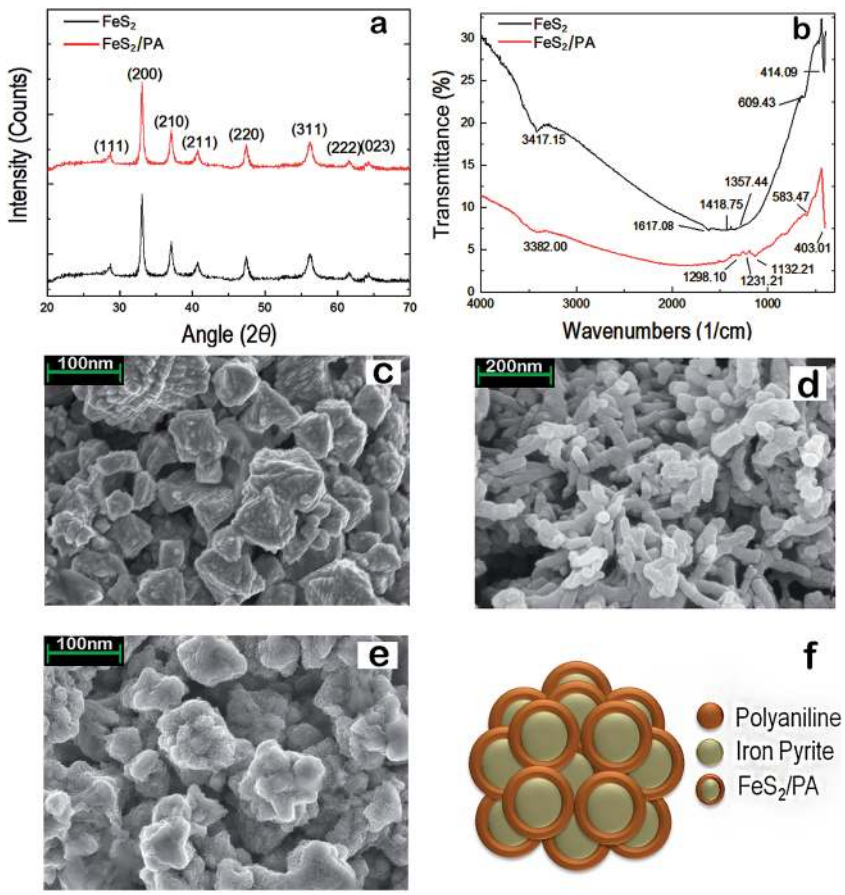

Fig. 2 Characterization of the electrode. (a) XRD of FeS_2 and FeS_2/PA. (b) FTIR of FeS_2 and FeS_2/PA. (c) SEM images of FeS_2 showed pseudo octahedral flowery morphology. (d) SEM image of PA showed rod or tubular morphology. (e) SEM images of FeS_2/PA have missing sharp feature of FeS_2, instead showed more globular morphology. (f) Poly-aniline encapsulation on the FeS_2 particles.

For the FeS_2/PA composite, band at 3380 cm^{-1} and 1530 cm^{-1} could be corresponding to O–H stretching and bending mode of water respectively. The band at 1420 cm^{-1} could be S–O stretching of sulfite species and 403 cm^{-1} would be disulfide (S–S) stretch. The band at the characteristic peaks at 1295 cm^{-1} and 1225 cm^{-1} could be corresponding to the quinoid ring (Q) and the benzene ring, respectively. The characteristic band of poly-aniline base will be the N=Q=N stretching band at 1128 cm^{-1}.[5,32–35] Raman spectrum was recorded in wave numbers ranging from 200 cm^{-1} to 500 cm^{-1} (ESI Fig. S3†). Sharp peaks were observed at 337 cm^{-1}, 378 cm^{-1}, and 431 cm^{-1}; which is in agreement with published Raman spectroscopic results for pure FeS_2 crystals.[32–35] From the XRD, Raman Spectroscopy and FTIR it could be concluded that synthesized FeS_2 possess single-phase pyrite without detectable marcasite, greigite, pyrrhotite, or other impurities. In SEM analysis of FeS_2, it exhibited a pseudo octahedral or flowery morphology with an average particle diameter of 400–500 nm (Fig. 2c). We observed similar morphologies of FeS_2 nanostructures in our earlier work.[22,23] Fig. 2d provides the SEM image of the poly-aniline. The poly-aniline exhibited a rod or tubular morphology with an average thickness of 20–30 nm. Fig. 2e showed the representative SEM picture of FeS_2/PA composite. We observed that the sharp feature of FeS_2 is missing. Instead we observed a more globular morphology. It seems as if the poly-aniline has encapsulated the FeS_2 particles and offered them a more smooth and rounded texture and morphology respectively. Thus we have speculated that PA is forming a coating on the FeS_2 surface thereby enhancing the electrochemical activity/conductivity of the composite (Fig. 2f).

2.5. Electrochemical characterization of the device

The electrochemical characterization of the device was performed using electrochemical work station 'Epsilon BASi Cell Stand C3'. The charge–discharge measurements were performed using AutolabB.V (Metrohm). The working electrode was of FeS_2/PA with 1 cm^2 area which was sprayed on one side of the graphite sheet. Only FeS_2/PA area was activated as an electrode, remaining graphite sheet was kept as electrochemically insulated. The reference electrode was an Ag/AgCl (in 3 mol l^{-1} NaCl) electrode and the counter electrode was a platinum wire. CV was done at different scan rate from 5 mV s^{-1} to 300 mV s^{-1} at 0 to 0.8 V voltage window in aqueous 2 M H_3PO_4 solution.

3. Results and discussion

3.1. Rational for developing FeS_2/PA composite electrode and gel electrolyte

The two electrodes were prepared by a FeS_2/poly-aniline (PA) composite. Our rational for developing FeS_2/PA composite electrode is the following: PA has been extensively studied as cathode material for electrochemical capacitor due to its excellent conductivity, redox reversibility and its stability towards environment.[3,5,36–43] But one of the major drawbacks of using PA as stand alone electrode in the charge storage device is its poor discharge capacity.[38,39,42] On the other hand iron disulfide (FeS_2), one of the most abundant metal sulfide found on earth's crust, have three basic properties which are of immense significance for developing charge storage devices[19–21,40,41,44,45] *viz.*, (a) mediating electron-transfer (b) electrical-charge separation, (c) capability to store energy temporarily or in the form of stable chemical products. Here we have shown that using a low temperature strategy we could obtain uniform size particles of FeS_2. Thus marrying FeS_2 with PA in the form of a composite could offer added benefit in terms of charge storage and discharge potential. That inspired us to create FeS_2/poly-aniline composite. Further CV analysis showed that this strategy indeed mutually improved the charge storage and discharge capacity of both FeS_2 and PA. Further it has been observed that the presence of nanoparticles in the matrix of the conducting polymer results in enhanced electrochemical activity/conductivity.[43] The rational for choosing gel electrolyte was to ensure that the solution does not dry out easily and offer more flexibility to the device. The H_3PO_4 is reasonably biocompatible and also functions as an ionic liquid. Poly-vinyl alcohol (PVA) acts as a polymeric matrix thus simultaneously allowing ionic transport and functioning as a separator layer between the electrodes.[46]

3.2. Cyclic voltammetry (CV) analysis of the FeS_2, PA & FeS_2/PA electrodes and reason to select FeS_2/PA for developing the device

To evaluate the electrochemical performance of the FeS_2, PA and FeS_2/PA electrodes, cyclic voltammetry was carried out using Epsilon Basi C3 cell stand with conventional three electrode configuration in 2 M aqueous solution of H_3PO_4. CV was done at different scan rate from 5 mV s^{-1} to 300 mV s^{-1} at 0 to 0.8 V voltage window. Cyclic voltammogram of FeS_2/PA had approximately rectangular shape as compared to the FeS_2 and PA alone (Fig. 3a–c). FeS_2/PA showed higher specific capacitance, as compared to FeS_2 and PA alone. When the integrated area from CV from the voltammogram of FeS_2, PA and FeS_2/PA, we observed that FeS_2/PA covers 14 times higher area as compared to FeS_2 and 7 times higher area as compared to PA, thus highlighting the fact that FeS_2/PA has highest specific capacitance as compared to the individual components (Fig. 3d). Correspondingly the current density was almost 15 times higher in FeS_2/PA as compared to FeS_2 alone and 2 times higher than PA (at a scan rate of 300 mV s^{-1}) (Fig. 3d). Another interesting aspect of the CV of FeS_2 is the following: in Fig. 3a we observed a significant hump at 0.2 and 0.4 V thus indicating that certain redox reaction is taking place, thus resulting in the pseudo capacitance as well as double layer capacitance. In Fig. 3b, in CV of PA, we observed that there is no hump but the area of curve and peak current is significantly higher than FeS_2. Surprisingly in phosphoric acid environment, PA is not exhibiting observable pseudo-capacitance, whereas double layer capacitance is distinctly observable.[39,42,46] Now in the Fig. 3c and d, CV of FeS_2/PA showed small humps at 0.2 and 0.4 V, thus hinting at the occurrence of redox reaction. The FeS_2/PA has specific capacitance approximately 362 F g^{-1} m^{-1} whereas the

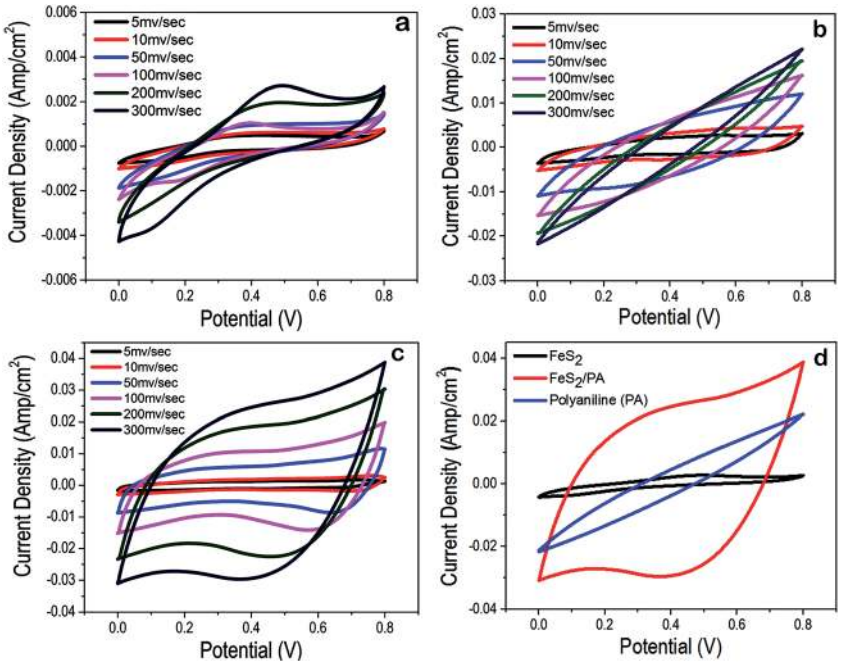

Fig. 3 CV analysis of electrode material. (a) CV of FeS_2 at different scan rates. (b) & (c) CV of PA and FeS_2/PA at same scan rates as seen in FeS_2. (d) Comparison of the specific capacitance of FeS_2 and FeS_2/PA through CV at 300 mV s^{-1} scan rate.

FeS_2 have 112 F g^{-1} m^{-1}. Thus addition of PA along with FeS_2 improves the electrochemical properties of the electrode. Now, on the basis of the CV analysis, it was clear that FeS_2/PA could perform as a better charge storage module as compared to FeS_2 and PA alone. Thus we fabricated a FeS_2/PA hybrid device and performed an electrochemical and charge/discharge characterization of the device (Fig. 4).

3.3. Electrochemical analysis of charge storage device

Further, cyclic voltammogram the charge storage device of FeS_2/PA was performed. CV at different scan rate from 100 mV s^{-1} to 300 mV s^{-1} and 0 to 0.8 V voltage window showed that the graph was almost rectangular in all scan rates and current density was

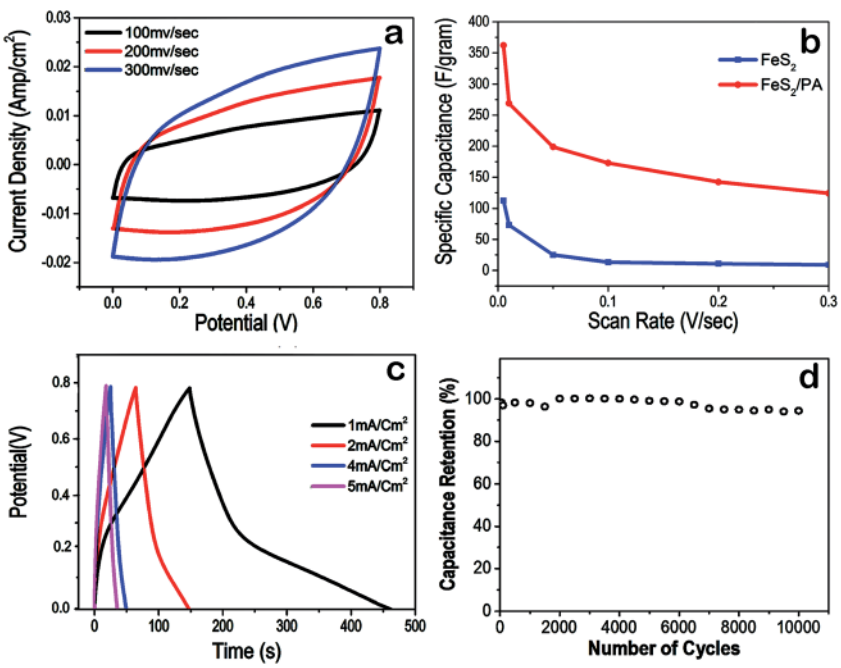

Fig. 4 Device characterization (a) CV of the device at different scan rate. (b) Relation between scan rate and specific capacitance. (c) Charge–discharge cycle of FeS_2/PA device at different current density. (d) Percentage capacitance retention *vs.* number of cycles to validate stability and performance of the prototype device till 10 000 charge–discharge cycles.

approximately 0.025A cm^{-2} for 300 mV s^{-1} (Fig. 4a). The specific capacitance (C_s) were calculated from the CV curves by equation

$$(C_s = \int I(u)\mathrm{d}t/m \times v \times \Delta V)$$

where, m indicates the mass of the active electrode material, I is the oxidation or reduction current, v is the scan rate, dt is time differential, and ΔV indicates the voltage range of one sweep segment.[6] It is observed that the specific capacitance decreased with an increase in the scan rate from 5 mV s^{-1} to 500 mV s^{-1} (Fig. 4b). This is possibly due to the insufficient time available for ion diffusion at faster scan rate. Galvanostatic charge–discharge characteristics of the device were performed using Autolab (NOVA 1.10 interface) at different current densities (1 mA cm^{-2}, 2 mA cm^{-2}, 4 mA cm^{-2} and 5 mA cm^{-2}). The observed discharge curves of the device exhibited an almost mirror symmetry with its charge counterpart at higher current density such as 5 mA cm^{-2} (Fig. 4c). Interestingly as the current density decreased, the charge time became less and discharge time became high as could be seen in 1 mA cm^{-2} curve. In terms of values, the charge and discharge time is same for 5 mA cm^{-2} that is 20 s but for 1 mA cm^{-2} the charging time is 160 seconds but the discharging time 310 seconds. This means that the device could store charges for longer period of time. The thing which is noteworthy was that for low current density (4 mA cm^{-2} downwards), the discharge curve shows some flatness after 0.25 to 0.3 V. This flatness indicates that the charge storage device could hold charge in usable voltage range for a significant amount of time. The specific capacitance for the electrodes could be obtained from charge–discharge data by equation

$$(C = I \times \Delta t/m \times \Delta V),$$

where C (F g^{-1}) is the specific capacitance, I (A) is the constant discharging current, Δt (s) is the discharging time, ΔV (V) is the potential window, and m (g) is the mass loading of the active material in the working.[6] The specific capacitances of the FeS_2/PA electrode are 390, 220, 125 and 113 F g^{-1} at the current densities of 1, 2, 4 and 5.0 mA cm^{-2}, respectively. It can be seen here, that the specific capacitance values decreased with increasing current density.

3.4. Evaluating the functional stability of the electrodes and the device

Three methods were employed to verify the long term stability of the device. First, a 10 000 charge/discharge cycles at a fixed current density of 1 mA cm^{-2} was used to verify the long term capacitance retention property of the device (Fig. 4d) and cyclic voltammetry of FeS_2/PA electrode at 300 mV s^{-1} scan rate to verify the long term cycling stability (Fig. 5a). We observed that after 10 000 charge/discharge cycles, the charge storage in the device was at 97% of the maximum storage capability. Similar electrochemical stability was observed after conducting 10 000 cycles of CV using the FeS_2/PA electrode material. It should be noted from Fig. 5b that the current density was still at 40 mA cm^{-2}, which is about 95% of the initial value; demonstrating the long term cyclic stability of the device prototype. Further we made a comparative CV analysis of fresh FeS_2/PA electrode with FeS_2/PA electrodes treated continuously with H_3PO_4 (pH 1.4, 2 M H_3PO_4 aqueous solution) for two, four and seven days

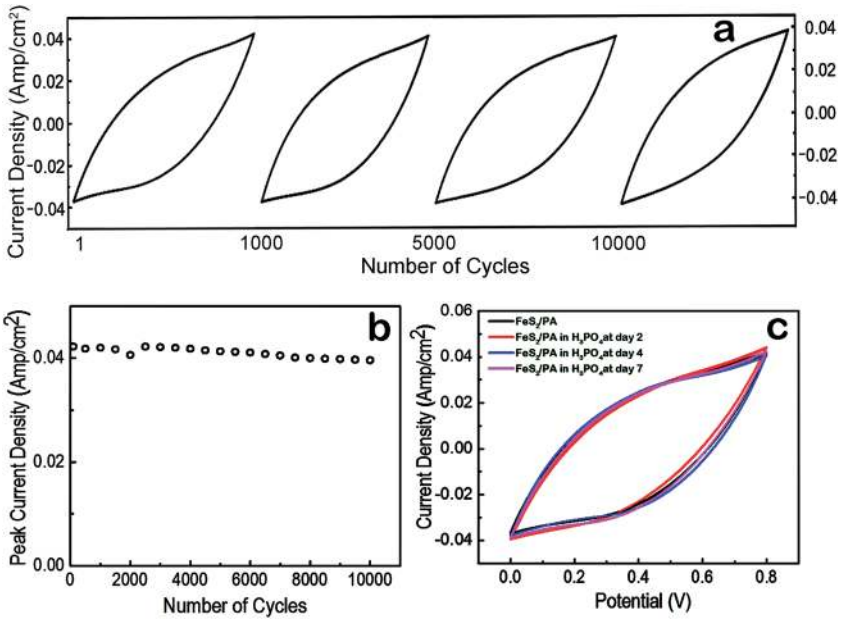

Fig. 5 Functional stability experiment. (a) CV cycles comparison for shape and storage capability retention from first to ten thousand cycle indicating that current density of 0.04 A cm^{-2} is maintained throughout. (b) Peak current density following 10 000 cycles was maintained at 0.04 A cm^{-2} c^{-1}. CV comparison of fresh FeS_2/PA electrode with FeS_2/PA electrodes treated with H_3PO_4 for two, four and seven days respectively demonstrating similar current density and shape.

respectively demonstrating similar current density and shape (Fig. 5c).

3.5. Evaluating the structural stability of the electrode material used in the device

We conducted two experiments to establish the structural stability of FeS_2/PA material in H_3PO_4 environment (pH 1.21–1.4). First, freshly prepared samples of FeS_2 (100 mg each) was kept in 1.4 pH 5 ml 2 M H_3PO_4 for two, four, and seven days in three different vials. After completing the second, fourth and seventh day respectively; FeS_2 was taken out from the vials, and conducted XRD and SEM investigation on those samples. Same experiment was conducted for the FeS_2/PA material. The XRD graph in Fig. 6 exhibits the same peaks for all samples for each specific day for both FeS_2 and FeS_2/PA materials. We did not observe any difference in the XRD peaks and further we observed similar morphology in the SEM analysis as shown in Fig. 7; thus demonstrating the stability of the material even after seventh day in H_3PO_4 environment.

3.6. Testing the efficacy of the device

Initially the device had to be charged using a 2 V DC power source. For optimal efficiency of the device, the first charging should be done approximately for 1 hour. Then onward, subsequent charging need not require more than 5 minute. Once the device was fully charged, three devices are connected in a series circuit, which is sufficient to glow an light emitting diode (LED) device for more than 1 hour (ESI video file 1†) and could operate a simple electrical motor (ESI video file 2†). The minimum voltage requirement of the LED was 1.6 V and 20 μA current. The device had a charge storage capacity of approximately 20 mA h and the maximum discharging current is 30 mA (device dimension 2 cm^2). If the size of the device was increased, then the discharge carrying capacity would subsequently increase, and it could run a DC motor, stepper motor *etc.* The

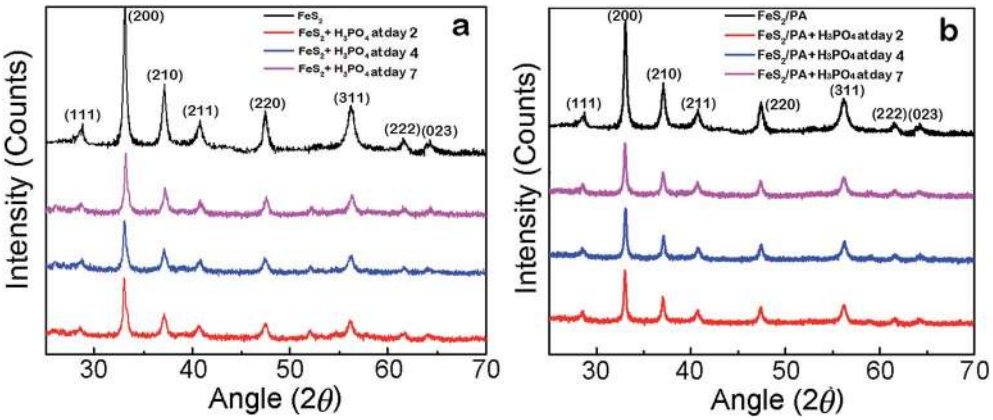

Fig. 6 Structural comparison (XRD). (a) XRD of FeS_2 at second, fourth and seventh day of H_3PO_4 treatment. (b) XRD of FeS_2/PA at second, fourth and seventh day of H_3PO_4 treatment.

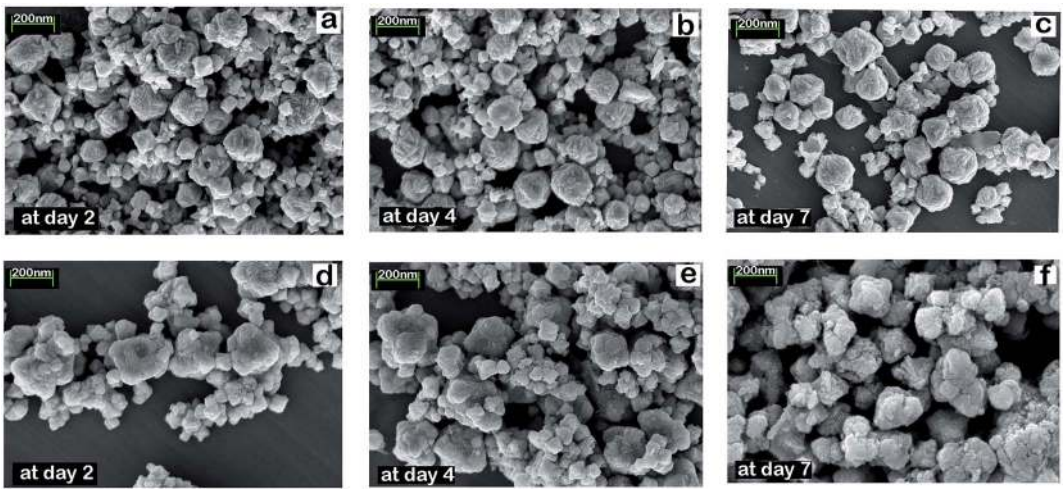

Fig. 7 SEM images of FeS_2 and FeS_2/PA nanoparticles after 2, 4 and 7 days of H_3PO_4 treatment (a) FeS_2 at day 2. (b) FeS_2 at day 4. (c) FeS_2 at day 7. (d) FeS_2/PA at day 2. (e) FeS_2/PA at day 4. (f) FeS_2/PA at day 7.

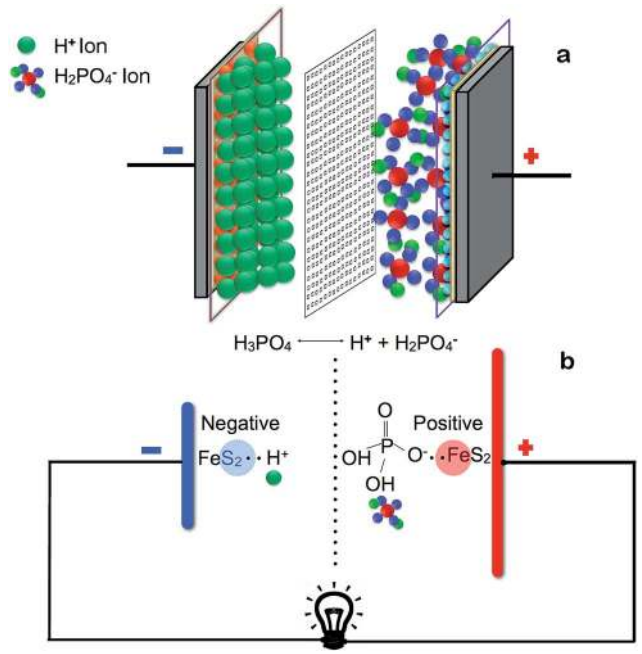

Fig. 8 Proposed charge storage mechanism of the device. (a) Electrical double layer formation during charging. The electrolyte (H_3PO_4) dissociates and H^+ ions migrate towards the cathode and $H_2PO_4^-$ ions migrate towards the anode. (b) Possible pseudo capacitive effects occur at the electrode surface. Since sulfur atom is a nucleophile having enough electron density, which will easily create an adduct with H^+ and thus possibly forming H–S hydrogen bonding. Whereas Fe center has enough positive character, so it can act as an electrophile, where it can create a loose electrostatic bonds with oxo donor group of phospho ion. In summary these features of nano FeS_2 offers it a bi-functional electrode character.

device could be more extremely flexible and foldable by coating of graphite on a cello-tape.

3.7. Proposed model of charge transfer and the overall discussion

The key question is how the proposed device stored electrical energy? There could be multiple strategies by which charge could be stored *viz.*, electrochemical double-layer capacitance, pseudo-capacitance, battery effects and other small capacitive effects.[47,48] The charge accumulation at the electrode–electrolyte interface generates electrochemical double-layer capacitance and possibly some pseudo-capacitance was generated due to certain faradic reaction on the electrode surface[6,8,49] (Fig. 8). Thus the total capacitance produced by the device was due to the addition of two capacitances along with the other small capacitive effects. Further the property of sulfur ions to work as electron sink and thus causing delocalized electronic states, might help in efficient electron transfer and optimal kinetics to run the device efficiently.[15,26–28,41,44] Further, the entrapment of FeS_2 nano particles in the conducting polymer matrix of PA possibly offers better electrochemical activity/conductivity.[43] The device which had been developed here is in its crudest form. If this is refined further, this could find several applications in the emerging domain of sustainable energy storage devices for flexible electronics.

4. Conclusions

In this work, we propose an innovative and novel application of nano FeS_2 *viz.*, as a symmetric charge storage device that is flexible, portable, light weight; along with its fabrication details. In its present laboratory prototype form; it powers solid-state electronic devices and electric motors. Further refinements of this device will open new avenues in the field of sustainable charge storage devices and low power electronics.

Acknowledgements

Acknowledgement This work is part of AD's doctoral thesis. AD is supported by MHRD, GOI. MR is supported by SB/FT/CS-199/2013 (DST- SERB, GOI).

References

1 H. Chen, T. N. Cong, W. Yang, C. Tan, Y. Li and Y. Ding, Science Direct Prog, *Nat. Sci.*, 2009, **19**, 291.
2 H. Ibrahim, A. Ilinca and J. Perron, *Renewable Sustainable Energy Rev.*, 2008, **12**, 1221.
3 Z. Song and H. Zhou, *Energy Environ. Sci.*, 2013, **6**, 2280.
4 H. Kim, J. Lee, H. Ahn, O. Kim and M. J. Park, *Nat. Commun.*, 2015, **6**, 7278.
5 D. Zang, J. P. Tu, Y. J. Mai, J. Zang, Y. Q. Quio and X. L. Wang, *J. Australas. Ceram. Soc.*, 2012, **2**, 189.
6 Z. Li, Z. Zhou, G. Yun, K. Shi, X. Lv and B. Yang, *Nanoscale Res. Lett.*, 2013, **8**, 2.
7 X. H. Lu, D. Z. Zheng, T. Zhai, Z. Q. Liu, Y. Y. Huang, S. L. Xie and Y. X. Tong, *Energy Environ. Sci.*, 2011, **4**, 2915.
8 Q. Chen, X. Li, X. Zang, Y. Cao, Y. He, P. Li, K. Wang, J. Wei, D. Wud and H. Zhu, *RSC Adv.*, 2014, **4**, 36253.
9 V. K. Thakur, G. Q. Ding, J. Ma, P. S. Lee and X. H. Lu, *Adv. Mater.*, 2012, **24**, 4071.
10 Y. Wang and W. H. Zhong, *ChemElectroChem*, 2015, **2**, 22.
11 D. Larcher and J.-M. Tarascon, *Nat. Chem.*, 2015, **7**, 19.
12 I. Hadjipaschalis, A. Poullikkas and V. Efthimiou, *Renewable Sustainable Energy Rev.*, 2009, **13**, 1513.
13 C. Schaber, P. Mazza and R. Hammerschlag, *Electricity Journal*, 2014, **05**, 21.
14 A. Andrijanovits, H. Hoimoja and D. Vinnikov, *Elektron. Elektrotech.*, 2012, **118**, 21.
15 M. Lee, G. P. Kim, H. D. Song, S. Park and J. Yi, *Nanotechnology*, 2014, **25**, 345601.
16 K. Bradbury, *Energy storage technology review*, Duke University, 2010, pp. 1–34, http://people.duke.edu/~kjb17/tutorials/Energy_Storage_Technologies.pdf.
17 A. Manthiram, A. V. Murugan, A. Sarkar and T. Muraliganth, *Energy Environ. Sci.*, 2008, **1**, 621.
18 R. T. Lowson, *Chem. Rev.*, 1982, **82**, 461.
19 D. Rickard and G. W. Luther III, *Chem. Rev.*, 2007, **2**, 514.
20 Y. N. Zhang, J. Hu, M. Law and R. Q. Wu, *Phys. Rev. B: Condens. Matter Mater. Phys.*, 2012, **85**, 085314.

21 P. P. Altermatt, T. Kiesewetter, K. Ellmer and H. Tributsch, *Sol. Energy Mater. Sol. Cells*, 2002, **2**, 71.
22 G. Srivastava, A. Das, T. S. Kusurkar, M. Roy, S. Airan, R. K. Sharma, S. K. Singh, S. Sarkar and M. Das, *Mater. Express*, 2014, **4**, 23.
23 G. Srivastava, C. K. Das, A. Das, S. K. Singh, M. Roy, H. Kim, N. Sethy, A. Kumar, R. K. Sharma, S. K. Singh, D. Philip and M. Das, *RSC Adv.*, 2014, **4**, 58495.
24 L. Zhu, B. J. Richardson and Q. Yu, *Nanoscale*, 2014, **6**, 1029.
25 M. Das, G. Srivastava, C. Das, A. Dubey, N. Sethy, K. Bhargava, S. K. Singh and D. Philip, *New AG International India*, June 2015, pp. 41–42.
26 H. Tributsch, *Sulfur Its Significance for Chemistry, for the Geo-Bio- and Cosmosphere and Technology*, ed. A. Müller and B. Krebs, Elsevier Science Publishers, 1984.
27 T. A. Bither, R. J. Bouchard, W. H. Cloud, P. C. Donohue and W. J. Siemons, *Inorg. Chem.*, 1968, **7**, 2208.
28 H. S. Jarret, W. H. Cloud, R. J. Bouchard, S. R. Butler, C. G. Frederick and J. L. Gillison, *Phys. Rev. Lett.*, 1968, **21**, 617.
29 Y. Wang, H. Liao, J. Wang, X. Qian, Y. Zhu and S. Cheng, *Int. J. Electrochem. Sci.*, 2013, **8**, 4002.
30 K. Lee, S. Cho, S. H. Park, A. J. Heeger, C.-W. Lee and S.-H. Lee, *Nature*, 2006, **441**, 65–68.
31 H. Lin, L. Li, J. Ren, Z. Cai, L. Qiu, Z. Yang and H. Peng, *Sci. Rep.*, 2013, **3**, 1353.
32 M. Y. C. Teo, S. A. Kulinich, O. A. Plaksin and A. L. Zhu, *J. Phys. Chem. A*, 2010, **114**, 4173.
33 Y. Bi, Y. Yuan, C. L. Exstrom, S. A. Darveau and J. Huang, *Nano Lett.*, 2011, **11**, 4953.
34 X. Qiu, M. Liu, T. Hayashi, M. Miyauchi and K. Hashimoto, *Chem. Commun.*, 2013, **49**, 1232.
35 W. L. Liu, X. H. Rui, H. T. Tan, C. Xu, Q. Y. Yan and H. H. Hng, *RSC Adv.*, 2014, **4**, 48770.
36 Y. K. Zhou, B. L. He, W. J. Zhou, J. Huang, X. H. Li, B. Wu and H. L. Li, *Electrochim. Acta*, 2004, **49**, 257.
37 Y. Liao, C. Zhang, Y. Zhang, V. Strong, J. Tang, X. G. Li, K. K. Zadeh, E. M. V. Hoek, K. L. Wang and R. B. Kaner, *Nano Lett.*, 2011, **11**, 954.
38 M. Khalid, M. A. Tumelero and A. A. Pasa, *RSC Adv.*, 2015, **5**, 62033.
39 C. Y. Wang, V. Mottaghitalab, C. O. Too, G. M. Spinks and G. G. Wallace, *J. Power Sources*, 2007, **163**, 1105.
40 X. Rui, H. Tan and Q. Yan, *Nanoscale*, 2014, **6**, 9889.
41 Y. Zhu, L. Suo, T. Gao, X. Fan, F. Han and C. Wang, *Electrochem. Commun.*, 2015, **54**, 18.
42 R. Pauliukaite, C. M. Brett and A. P. Monkman, *Electrochim. Acta*, 2004, **50**, 159.
43 C. Karunakaran, P. Santharaman and M. Das, Biosensors and Bioelectronics, *Nanocomposite Matrix Functionalization for Biosensors*, ed. C. Karunakaran, R. Rajkumar and K. Bhargava, Elsevier, 2015, pp. 69–132.
44 A. Ennaoui, S. Fiechter, C. Pettenkofer, N. Alonso-Vante, K. Buker, M. Bronold, Ch. Hopfner and H. Tributch, *Sol. Energy Mater. Sol. Cells*, 1993, **29**, 289.
45 T. P. Dhakal, L. K. Ganta, D. Van Hart, C. R. Westgate, Annealing of FeS_2 nano-crystal thin film, in *Photovoltaic Specialists Conference (PVSC)*, 2012, 38th IEEE, pp. 000170–000173, DOI: 10.1109/PVSC.2012.6317593.
46 L. Viliciauskas, M. E. Tuckerman, G. Bester, S. J. Paddison and K. D. Kreuer, *Nat. Chem.*, 2012, **4**, 461.
47 Z. Qin, Z. J. Li, M. Zhang, B. C. Yang and R. A. Outlaw, *J. Power Sources*, 2012, **217**, 303.
48 J. Bae, M. K. Song, Y. J. Park, J. M. Kim, M. L. Liu and Z. L. Wang, *Angew. Chem., Int. Ed.*, 2012, **51**, 4934.
49 J. T. Zhang, J. W. Jiang, H. L. Li and X. S. Zhao, *Energy Environ. Sci.*, 2011, **4**, 4009.